

Damped spin-excitations in a doped cuprate superconductor with orbital hybridization

O. Ivashko,¹ N. E. Shaik,² X. Lu,³ C. G. Fatuzzo,² M. Dantz,³ P. G. Freemann,⁴
 D. E. McNally,³ D. Destraz,¹ N. B. Christensen,⁵ T. Kurosawa,⁶ N. Momono,^{6,7}
 M. Oda,⁶ C. Monney,¹ H. M. Rønnow,² T. Schmitt,³ and J. Chang^{1,*}

¹Physik-Institut, Universität Zürich, Winterthurerstrasse 190, CH-8057 Zürich, Switzerland

²Institute for Condensed Matter Physics, École Polytechnique Fédérale de Lausanne (EPFL), CH-1015 Lausanne, Switzerland

³Swiss Light Source, Paul Scherrer Institut, CH-5232 Villigen PSI, Switzerland

⁴Jeremiah Horrocks Institute for Mathematics, Physics and Astronomy,
 University of Central Lancashire, PR1 2HE Preston, United Kingdom

⁵Department of Physics, Technical University of Denmark, DK-2800 Kongens Lyngby, Denmark.

⁶Department of Physics, Hokkaido University - Sapporo 060-0810, Japan

⁷Department of Applied Sciences, Muroran Institute of Technology, Muroran 050-8585, Japan

A resonant inelastic x-ray scattering (RIXS) study of overdamped spin-excitations in slightly underdoped $\text{La}_{2-x}\text{Sr}_x\text{CuO}_4$ (LSCO) with $x = 0.12$ and 0.145 is presented. Three high-symmetry directions have been investigated: (1) the anti-nodal $(0,0) \rightarrow (1/2,0)$, (2) the nodal $(0,0) \rightarrow (1/4,1/4)$ and (3) the zone boundary direction $(1/2,0) \rightarrow (1/4,1/4)$ connecting these two. The overdamped excitations exhibit strong dispersions along (1) and (3), whereas a much more modest dispersion is found along (2). This is in strong contrast to the un-doped compound La_2CuO_4 (LCO) for which the strongest dispersions are found along (1) and (2). The $t - t' - t'' - U$ Hubbard model used to explain the excitation spectrum of LCO predicts – for constant U/t – that the dispersion along (3) scales with $(t'/t)^2$. However, the diagonal hopping t' extracted on LSCO using single-band models is low ($t'/t \sim -0.16$) and decreasing with doping. We therefore invoked a two-orbital ($d_{x^2-y^2}$ and d_{z^2}) model which implies that t' is enhanced and that the Coulomb interaction U is renormalized. Both these effects act to enhance the zone boundary dispersion within the Hubbard model. We thus conclude that hybridization of $d_{x^2-y^2}$ and d_{z^2} states has a significant impact on the zone boundary dispersion in LSCO.

I. INTRODUCTION

Considerable research is being undertaken in the quest to reach consensus on the mechanism of high-temperature superconductivity¹ and the associated pseudogap phase² in copper-oxide materials (cuprates). The energy scales governing the physical properties of these layered materials therefore remain of great interest. It is known that these materials are characterized by a strong super-exchange interaction $J_1 = 4t^2/U$ where t is the nearest-neighbor hopping integral and U is the Coulomb interaction. To first order, this energy scale sets the band-width of the spin-excitation spectrum. Resonant inelastic x-ray scattering (RIXS) experiments³ have demonstrated that this band-width stays roughly unchanged across the entire phase diagram^{4,5} of hole doped cuprates. It has also been demonstrated that the cuprates belong to a regime (of t and U) where the second order exchange-interaction $J_2 = 4t^4/U^3$ contributes to a spin-excitation dispersion along the antiferromagnetic zone boundary (AFZB)⁶⁻⁹. Moreover, it is known from band structure calculations and experiments that the next nearest-neighbor (diagonal) hopping integral t' constitutes a non-negligible fraction of t ¹⁰. Empirically¹¹, the superconducting transition scales with the ratio t'/t whereas Hubbard type models predict the opposite trend^{12,13}. As a resolution, a two-orbital model – in which hybridization of d_{z^2} and $d_{x^2-y^2}$ states suppresses T_c and enhances t' – has been put forward¹⁴.

Here, we address the question as to how t' influences

the spin-excitation spectrum at, and in vicinity to, the antiferromagnetic zone boundary. We have therefore studied – using the RIXS technique – slightly underdoped compounds of $\text{La}_{2-x}\text{Sr}_x\text{CuO}_4$ (LSCO) with $x = 0.12$ and 0.145 . Even though the system is not antiferromagnetically ordered at these dopings, we quantify the zone boundary dispersion $\omega(k)$ by $E_{ZB} = \omega(1/2,0) - \omega(1/4,1/4)$. In doped LSCO a strongly enhanced zone boundary dispersion is observed. As will also be shown, within the $t - t' - t'' - U$ Hubbard model, one generally expects that the zone boundary dispersion scales with t'/t with a prefactor that depends on U/t . The Fermi surface topology of LSCO, obtained from photoemission spectroscopy and analyzed with a single-band tight binding model, suggests that t' decreases with increasing doping^{10,15}. The Hubbard model is thus within a single-band picture not consistent with the experiment. However, using a two-orbital model, in which hybridization between d_{z^2} and $d_{x^2-y^2}$ states enhances t' ¹⁴ and yields a lower effective Coulomb interaction U . Combined this provide ingredients to a satisfactory description of the zone boundary dispersion. We thus conclude that the two-orbital model¹⁴ is necessary to understand the spin-excitation spectrum of doped LSCO.

II. METHOD

The RIXS experiment was carried out at the ADvanced RESonant Spectroscopies (ADRESS) beamline^{16,17} at

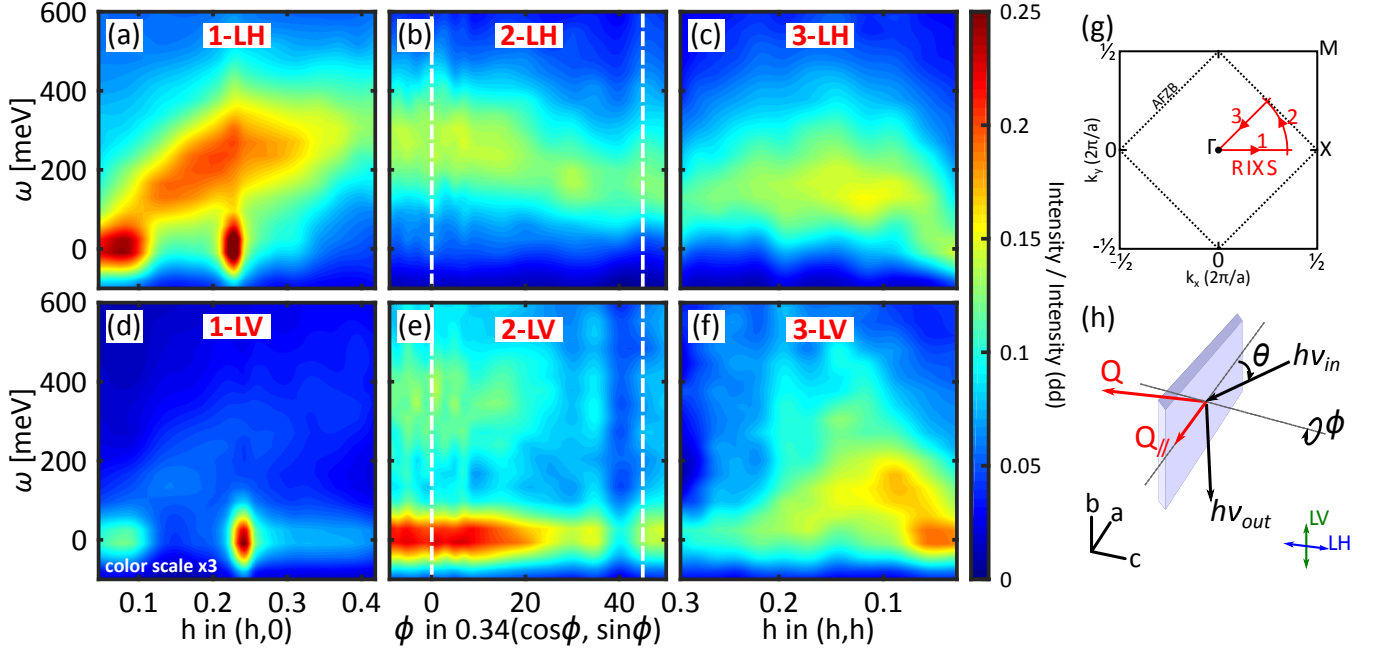


FIG. 1. (Color online) RIXS spectra versus momentum recorded on $\text{La}_{2-x}\text{Sr}_x\text{CuO}_4$ with $x = 0.12$ under grazing exit conditions and displayed in false color scale for different light polarizations. (a,d) RIXS intensity maps along the anti-nodal direction for linear-horizontal and linear-vertical incident light polarizations. (c,f) similar maps but along the nodal direction. (b,e) azimuthal RIXS maps connecting nodal and anti-nodal directions as shown schematically in (g). Consistent with what has previously been shown the spin-excitation matrix element is strongest for the LH polarization. By contrast, the charge-density-wave reflection at $Q_{\text{CDW}} = (\pm\delta_1, \delta_2)$ with $\delta_1 \sim 0.23$ and $\delta_2 \sim 0.01$ is about three times more intense with LV polarization. (g) shows the scan directions with respect to the antiferromagnetic zone boundary (AFZB). (h) displays the scattering geometry where θ indicates the incident angle and ϕ is the azimuthal angle. Varying these angles allows to scan the in-plane momentum $Q_{||}$.

the Swiss Light Source (SLS) with the geometry shown in Fig. 1(h). The newly installed CARVING RIXS manipulator allowed to probe the full kinematically accessible reciprocal space (h, k) with a scattering angle of 130° . Incident photons with an energy of 933 eV (at the Cu L_3 -edge resonance) gave an instrumental energy and momentum resolution of 132 meV and 0.01 \AA^{-1} respectively. Both the linear horizontal (LH) and linear vertical (LV) light polarizations were applied to probe high quality single crystals of $\text{La}_{2-x}\text{Sr}_x\text{CuO}_4$ with $x = 0.12$ and 0.145 ($T_c = 27$ and 35 K respectively). These crystals were grown by the traveling floating zone method¹⁸ and previously characterized in neutron^{19–21} and μSR ²² experiments. Ex-situ pre-alignment of the samples was carried out using a Laue diffractometer. The samples were cleaved in-situ using a standard top-post technique and all data were recorded at $T = 20 \text{ K}$. Although being in the low temperature orthorhombic (LTO) crystal structure, tetragonal notation $a \cong b \approx 3.78 \text{ \AA}$ ($c \approx 13.2 \text{ \AA}$) is adopted to describe the in-plane momentum (h, k) in reciprocal lattice units $2\pi/a$.

III. RESULTS

Fig. 1(a-c) displays grazing exit RIXS spectra of $\text{La}_{1.88}\text{Sr}_{0.12}\text{CuO}_4$ recorded with incident LH light polarization along three trajectories as indicated in (g). Data along the same directions but measured with incident LV polarization are shown in (d-f). Besides the strong elastic scattering found at the specular condition [$Q = (0, 0)$], an elastic charge-density-wave (CDW) reflection is found – consistent with existing literature^{23,24} – along the $(h, 0)$ direction at $Q = (\delta_1, \delta_2)$ with $\delta_1 = 0.23(3)$ and $\delta_2 \simeq 0.01$. The charge order reflection serves as a reference point, demonstrating precise alignment of the crystal.

For grazing exit geometry, it has previously been demonstrated that spin-excitations are enhanced in the LH-channel⁴. In Fig. 2(a,b), selected raw RIXS spectra recorded with LH polarization are shown for momenta near the $(1/2, 0)$ and $(1/4, 1/4)$ points. The low-energy part of the spectrum consists of three components: a weak elastic contribution, a smoothly varying background and a damped spin-excitation. It is immediately clear that the excitations near $(1/4, 1/4)$ are significantly softened compared to those observed around the $(1/2, 0)$ -point (see Fig. 2(a,b)).

For a more quantitative analysis of the magnon dis-

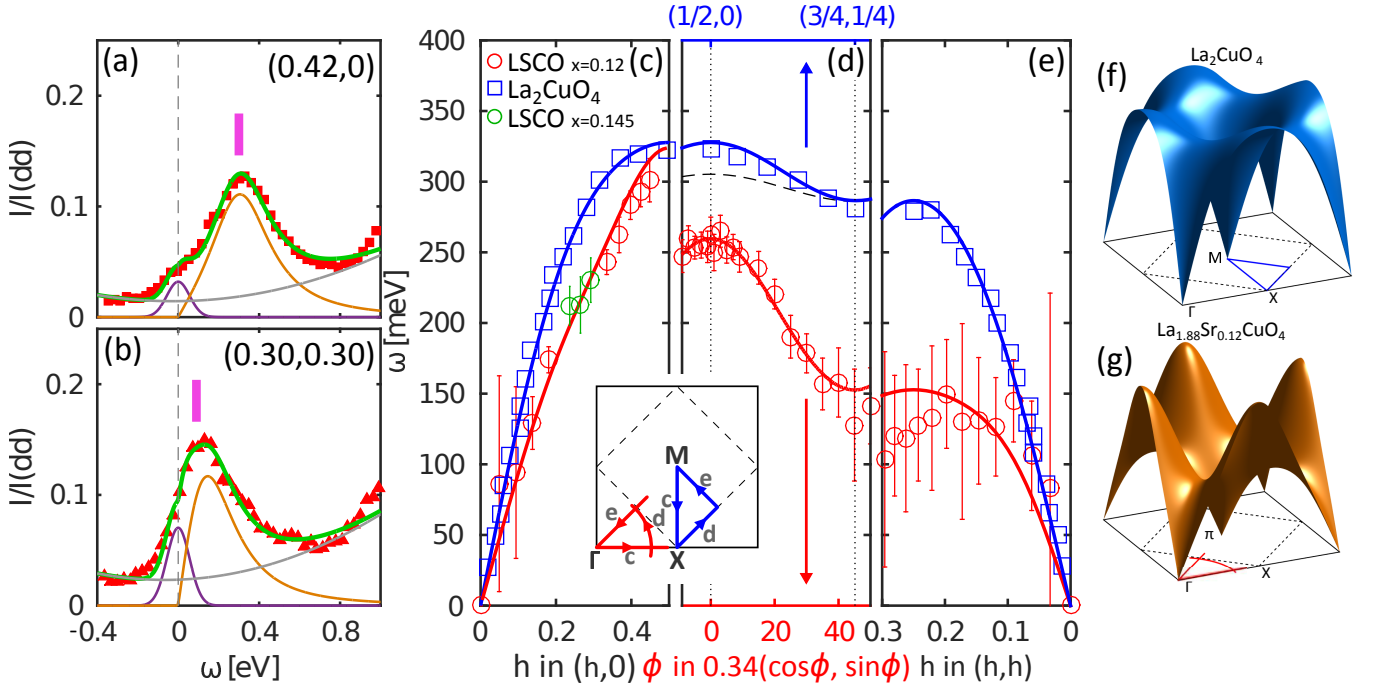


FIG. 2. (Color online) RIXS spectra for anti-nodal (a) and nodal (b) directions with the indicated in-plane momentum. The fit (solid green curve) is composed of three components: elastic line (purple), spin-excitation (orange) modeled by an anti-symmetric Lorentzian function and a quadratic background (grey) – see text for more detailed information. Vertical bars indicate the obtained poles of the Lorentzian function. (c)-(e) dispersion of the magnetic excitations in La_2CuO_4 (blue squares) and $\text{La}_{2-x}\text{Sr}_x\text{CuO}_4$ with $x = 0.12$ (red circles) observed by neutron scattering (Ref. 7) and RIXS (this work), respectively. Green circles in (c) are extracted from $\text{La}_{2-x}\text{Sr}_x\text{CuO}_4$ with $x = 0.145$ data. Within the antiferromagnetic zone scheme (indicated by the dashed line in the insert), red and blue cuts c and e are the equivalent anti-nodal and nodal directions. Solid lines in (c)-(e) are fits using a Heisenberg model, see text for further explanation. (f)-(g) schematic illustration of the spin-excitation dispersion in $\text{La}_{2-x}\text{Sr}_x\text{CuO}_4$ with $x = 0$ and $x = 0.12$, as indicated. In the doped compound, the spin-excitation dispersion is strongly renormalized along the diagonal (nodal, Γ -M) direction. Blue and red patterns indicate the experimentally measured high-symmetry directions.

persion, we modeled the elastic line with a Gaussian for which the standard deviation $\sigma = 56$ meV was set by the instrumental energy resolution. A second order polynomial function is used to mimic the background. Finally, to analyze the spin-excitations we adopted the response function of a damped harmonic oscillator^{4,25,26}:

$$\chi''(\omega) = \chi_0'' \frac{\gamma\omega}{(\omega^2 - \omega_0^2)^2 + \omega^2\gamma^2} = \frac{\chi_0''}{2\omega_1} \left[\frac{\gamma/2}{(\omega - \omega_1)^2 + (\gamma/2)^2} - \frac{\gamma/2}{(\omega + \omega_1)^2 + (\gamma/2)^2} \right],$$

where the damping coefficient $\gamma/2 = \sqrt{\omega_0^2 - \omega_1^2}$. The RIXS intensities are modeled by $[n_B(\omega) + 1] \cdot \chi''(\omega)$, where $n_B(\omega) = [\exp(\hbar\omega/k_B T) - 1]^{-1}$ is the Bose factor. As shown in Fig. 2(a-b), fitting to this simple model provides a good description of the observed spectra. In this fashion, we extracted the spin-excitation pole dispersion ω_1 (Fig. 2(c-e)) along the three trajectories shown in the insert. To avoid the influence of CDW ordering on the spin-excitation dispersion²⁷, we analyzed around the charge ordering vector spectra of LSCO $x = 0.145$ where

charge order is absent.

The extracted spin-excitation dispersion of LSCO $x = 0.12$ and 0.145 is to be compared with the magnon dispersion of the parent compound La_2CuO_4 ^{6,7,28,29}. Along the anti-nodal $(1/2, 0)$ -direction comparable dispersions are found. This is consistent with the weak doping dependence reported on LSCO⁵ and the $\text{YBa}_2\text{Cu}_3\text{O}_{7-\delta}$ (YBCO) system⁴. For the nodal $(1/4, 1/4)$ -direction, the dispersion of the doped compound is, however, strongly softened compared to La_2CuO_4 . Whereas this effect has been reported for Bi-based^{30,31} and overdoped LSCO²⁵, we demonstrate directly by an azimuthal scan how exactly this softening appears. Notice that the azimuthal dependence is closely related (but not exactly identical) to the scan along the antiferromagnetic zone boundary.

IV. DISCUSSION

A recent systematic study³² of un-doped cuprate compounds concluded that the zone boundary dispersion scales with the crystal field splitting $E_{x^2-y^2}$ of the $d_{x^2-y^2}$

and d_{z^2} states. Exact numerical determination of E_{z^2} is still a matter of debate³³. For a tetragonal system, E_{z^2} generally depends on the ratio between copper to apical d_{AO} and planar d_{PO} oxygen distances³⁴ (see insert of Fig. 3(a)). In underdoped LSCO, the crystal structure is orthorhombically distorted. This produces an in-plane (out-of-plane) distortion of the apical (in-plane) oxygen position. Here we argue that the in-plane distortion of the apical oxygen has approximately the same effect as if apical oxygen position would move further away from the CuO_2 plane. Therefore, we have in Fig. 3(a) added the in-plane distortion to d_{AO} . In this fashion, the ratio d_{AO}/d_{PO} decreases with increasing Sr content (Fig. 3(a))³⁵ in the LSCO system. From this doping dependence of d_{AO}/d_{PO} a gradual decrease of E_{z^2} is thus expected (Fig. 3(b))³⁴. Indeed, comparing the dd -excitations of LSCO $x = 0$ and 0.12 is consistent with a doping-induced shift of the d_{z^2} level (see Fig. 3(c,d)). In doped LSCO $x = 0.12$, we thus have a smaller crystal field splitting E_{z^2} than in undoped La_2CuO_4 . Yet, the zone boundary dispersion is larger in LSCO $x = 0.12$. Our experiment thus suggests that the zone boundary dispersion is not directly correlating with E_{z^2} .

The spin-excitation dispersion of doped LSCO is analyzed using an effective Heisenberg Hamiltonian derived from a $t - t' - t'' - U$ Hubbard model⁷⁻⁹. This discussion has three steps. First, an approximative analytical expression for the zone boundary dispersion is derived. Next, we compare to the experimentally obtained results using the known single-band tight-binding values of t, t' and t'' . It is shown that this approach is leading to unrealistically low values of the Coulomb interaction U . The d_{z^2} band is therefore included. This two-orbital scenario allows to describe the zone boundary dispersion with realistic input parameters, as presented in the last part of the discussion.

The simplest version of the Hubbard model contains only three parameters: the Coulomb interaction U , the band width ($4t$) and a renormalization factor Z – known to have little momentum dependence. To lowest order in $J_1 = 4t^2/U$, no magnon dispersion is expected along the zone boundary. Therefore, to explain the zone boundary dispersion – first observed on La_2CuO_4 – higher order terms $J_2 = 4t^4/U^3$ were included^{6,7} to the model. Later, it has been pointed out that higher order hopping terms t' and t'' can also contribute significantly^{8,9}. Generally, the effective Heisenberg model yields a dispersion^{8,9} $\omega(k) = Z\sqrt{A_k^2 - B_k^2}$ where A_k and B_k – given in the appendix – are depending on U, t, t' and t'' . The zone boundary dispersion can be quantified by $E_{ZB} = \omega(1/2, 0) - \omega(1/4, 1/4)$. Using the single-band Hubbard model with realistic parameters^{8,10,11} ($U/t \sim 8$, $|t'| \leq t/2$ and $t'' = -t'/2$) for hole doped cuprates, we

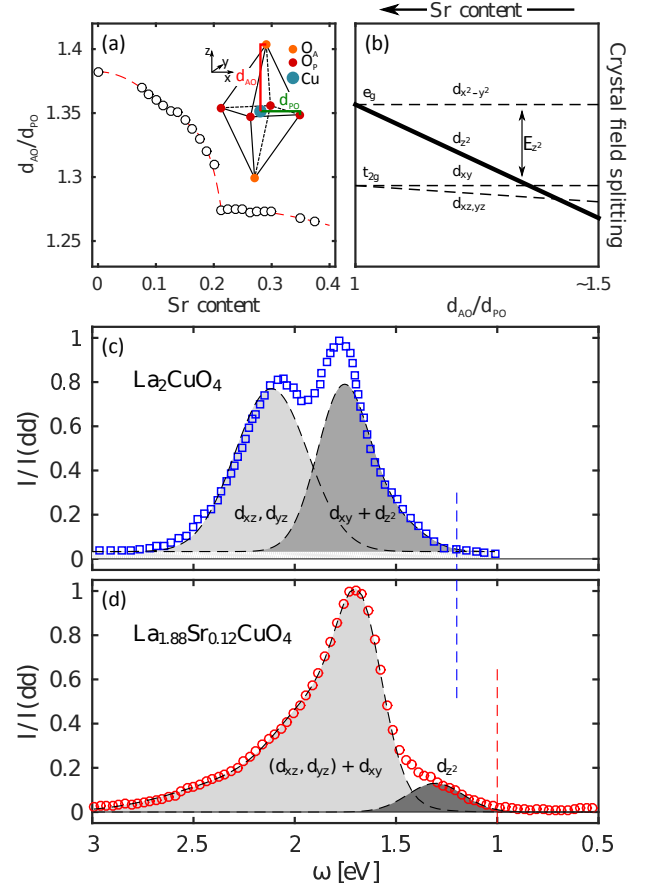


FIG. 3. (Color online) (a) Ratio d_{AO}/d_{PO} between copper to apical d_{AO} and planar d_{PO} oxygen distance. The apical oxygen distance is here set by adding its distance from the CuO_2 plane and its in-plane distortion from the copper position (see text for further explanation). Values of d_{AO}/d_{PO} are calculated from data given in Ref. 35. (b) Schematic of the crystal field splitting of the d -orbitals as a function of ratio d_{AO}/d_{PO} . As this ratio is reduced with doping, the d_{z^2} orbital is expected to soften. (c,d) RIXS spectra showing the dd -excitations for La_2CuO_4 (c) (adopted from Ref. 32) and $\text{La}_{1.88}\text{Sr}_{0.12}\text{CuO}_4$ (d) (this work). The grey shaded areas indicate schematically different orbital contributions. Vertical dashed lines display the onset of dd -excitations.

find (see appendix):

$$\frac{E_{ZB}}{12ZJ_2} \approx 1 + \frac{1}{12} \left[112 - \left(\frac{U}{t} \right)^2 \right] \left(\frac{t'}{t} \right)^2. \quad (1)$$

A key prediction is thus that E_{ZB} scales as $(t'/t)^2$ with a pre-factor that depends on $(U/t)^2$.

This effective Heisenberg model is in principle not applicable to doped and hence antiferromagnetic disordered cuprates. However, in the absence of alternative analytical models, it serves as a useful effective parametrization tool to describe the damped spin-excitations. Within a

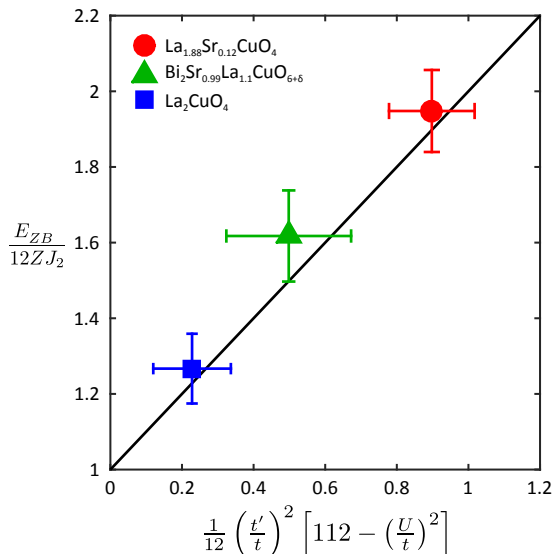


FIG. 4. (Color online) Experimentally obtained zone boundary dispersion E_{ZB} , normalized to $12ZJ_2$ – the expected theoretical value for $t' = t'' = 0$. To obtain J_2 the spin-excitation dispersion is fitted with U/t and t'/t as open parameters while keeping $t = 0.43$ eV, $t'' = -t'/2$ and $Z = 1.219$ fixed. Data points are obtained from fitting data on LSCO presented here (red circle) along with already published spin-excitation dispersions on LCO^{6,7} (blue square) and Bi2201³² (green triangle). Error bars stem from the standard deviations of the fitting parameters U/t and t'/t . The solid line is the predicted dependence of the $t-t'-t''-U$ Hubbard model with $U/t = 8$.

single-band tight-binding model, angle resolved photoemission spectroscopy (ARPES) experiments have found that t' decreases slightly with increasing doping^{10,15}. The stronger zone boundary dispersion can thus not be attributed to an increase of t' . Parameterizing the doping dependent zone boundary dispersion would thus imply a strong renormalization of U with increasing doping. For example, if we set $4t = 1720$ meV (obtained from LDA and ARPES^{11,36,37}) and $t'/t = -0.16$ and $t'' = -t'/2$, a fit yields $U/t \sim 4.7$ eV and $Z \sim 0.8$. Although these parameters provide a satisfactory description of the dispersion, the values of U and Z are not physically meaningful.

This failure combined with the observation of a reduced level splitting between the d_{z^2} and $d_{x^2-y^2}$ states (Fig. 3) motivates a two-band model. It has been demonstrated that d_{z^2} states contribute to effectively increase the t' hopping parameter¹⁴. Furthermore, with hybridization of d_{z^2} and $d_{x^2-y^2}$ states, a renormalized Coulomb interaction U is expected. Keeping $Z = 1.219$ as in La_2CuO_4 ⁸ and $t'' = -t'/2$, a satisfactory description (solid line in Fig. 2) of the spin-excitation dispersion is obtained for $t'/t = -0.38$ and $U/t = 6.5$. Notice that a similar ratio of t'/t has previously been inferred from the rounded Fermi surface topology of $\text{Ti}_2\text{Ba}_2\text{CuO}_{6+x}$,^{38,39} a

material for which the d_{z^2} states are expected to be much less important⁴⁰. It could thus suggest that $t'/t \approx -0.4$ is common to single layer cuprates but masked in LSCO due to the repulsion between the $d_{x^2-y^2}$ and d_{z^2} bands that pushes the van Hove singularity close to the Fermi level and effectively reshapes the Fermi surface topology¹⁴. The more realistic values of U and Z , suggest that – for LSCO – the two-orbital character of this system is an important ingredient to accurately describe the spin-excitation spectrum.

Once having extracted U/t and t'/t by fitting the experimental spin-excitation spectrum, we plot – in Fig. 4 – the normalized zone boundary dispersion $E_{ZB}/(12ZJ_2)$ versus $\frac{1}{12} (t'/t)^2 [112 - (U/t)^2]$. The same parameters were extracted (see Table I) from published RIXS data on La_2CuO_4 and $\text{Bi}_2\text{Sr}_{0.99}\text{La}_{1.1}\text{CuO}_{6+\delta}$ ³² and plotted in Fig. 4. All three compounds follow approximately the predicted correlation between $E_{ZB}/(12ZJ_2)$ and $\frac{1}{12} (t'/t)^2 [112 - (U/t)^2]$. This suggests that the zone boundary dispersion is controlled by the diagonal hopping t' and the coulomb interaction U .

Finally, we notice that recent RIXS experiments on LSCO thin films using SrLaAlO_4 (SLAO) substrates found a much less pronounced softening of the spin-excitation dispersion around the $(1/4, 1/4)$ -point⁴¹. A possible explanation is that LSCO films on SLAO have a larger c -axis lattice parameter and hence also a larger copper to apical-oxygen distance than what is found in bulk crystals^{42,43}. As a consequence, the d_{z^2} states are less relevant and a larger value of U is expected. This in turn would lead to a less pronounced zone boundary dispersion.

V. CONCLUSIONS

In summary, a comprehensive RIXS study of underdoped LSCO $x = 0.12$ and 0.145 were presented. The spin-excitation dispersion was studied along three high-symmetry directions and a strong zone boundary dispersion is reported. The spin-excitation dispersion was parametrized and discussed using a Heisenberg Hamiltonian derived from a Hubbard model including higher order hopping integrals. Within this model, the zone boundary dispersion scales with next nearest-neighbor hopping integral t'^2 . We argue that hybridization between d_{z^2} and $d_{x^2-y^2}$, which is especially strong in LSCO, leads to an enhanced t' and a renormalization of the Coulomb interaction U . Both these effects – consistent with the observations – lead to a stronger zone boundary dispersion within the $t-t'-t''-U$ Hubbard model.

VI. ACKNOWLEDGMENTS:

We acknowledge support by the Swiss National Science Foundation under grant number BSSGI0_155873 and

through the SINERGIA network Mott Physics beyond the Heisenberg Model. This work was performed at the ADRESS beamline of the SLS at the Paul Scherrer Institut, Villigen PSI, Switzerland. We thank the ADRESS beamline staff for technical support. M.D. and T.S.

have been partially funded by the Swiss National Science Foundation within the D-A-CH programme (SNSF Research Grant 200021L 141325). X.L. acknowledges financial support from the European Communitys Seventh Framework Program (FP7/2007–2013) under grant agreement NO. 290605 (COFUND: PSI-FELLOW).

-
- * johan.chang@physik.uzh.ch
- ¹ P. A. Lee, N. Nagaosa, and X.-G. Wen, *Rev. Mod. Phys.* **78**, 17 (2006).
 - ² M. R. Norman, D. Pines, and C. Kallin, *Advances in Physics* **54**, 715 (2005).
 - ³ L. J. P. Ament, M. van Veenendaal, T. P. Devereaux, J. P. Hill, and J. van den Brink, *Rev. Mod. Phys.* **83**, 705 (2011).
 - ⁴ M. L. Tacon, G. Ghiringhelli, J. Chaloupka, M. M. Sala, V. Hinkov, M. W. Haverkort, M. Minola, M. Bakr, K. J. Zhou, S. Blanco-Canosa, C. Monney, Y. T. Song, G. L. Sun, C. T. Lin, G. M. D. Luca, M. Salluzzo, G. Khaliullin, T. Schmitt, L. Braicovich, and B. Keimer, *Nat. Phys.* **7**, 725 (2011).
 - ⁵ M. P. M. Dean, G. Dellea, R. S. Springell, F. Yakhou-Harris, K. Kummer, N. B. Brookes, X. Liu, Y.-J. Sun, J. Strle, T. Schmitt, L. Braicovich, G. Ghiringhelli, I. Božović, and J. P. Hill, *Nat Mater* **12**, 1019 (2013).
 - ⁶ R. Coldea, S. M. Hayden, G. Aeppli, T. G. Perring, C. D. Frost, T. E. Mason, S.-W. Cheong, and Z. Fisk, *Phys. Rev. Lett.* **86**, 5377 (2001).
 - ⁷ N. S. Headings, S. M. Hayden, R. Coldea, and T. G. Perring, *Phys. Rev. Lett.* **105**, 247001 (2010).
 - ⁸ J.-Y. P. Delannoy, M. J. P. Gingras, P. C. W. Holdsworth, and A.-M. S. Tremblay, *Phys. Rev. B* **79**, 235130 (2009).
 - ⁹ B. Dalla Piazza, M. Mourigal, M. Guarise, H. Berger, T. Schmitt, K. J. Zhou, M. Grioni, and H. M. Rønnow, *Phys. Rev. B* **85**, 100508 (2012).
 - ¹⁰ T. Yoshida, X. J. Zhou, K. Tanaka, W. L. Yang, Z. Hussain, Z.-X. Shen, A. Fujimori, S. Sahrakorpi, M. Lindroos, R. S. Markiewicz, A. Bansil, S. Komiya, Y. Ando, H. Eisaki, T. Kakeshita, and S. Uchida, *Phys. Rev. B* **74**, 224510 (2006).
 - ¹¹ E. Pavarini, I. Dasgupta, T. Saha-Dasgupta, O. Jepsen, and O. K. Andersen, *Phys. Rev. Lett.* **87**, 047003 (2001).
 - ¹² S. R. White and D. J. Scalapino, *Phys. Rev. B* **60**, R753 (1999).
 - ¹³ T. Maier, M. Jarrell, T. Pruschke, and J. Keller, *Phys. Rev. Lett.* **85**, 1524 (2000).
 - ¹⁴ H. Sakakibara, H. Usui, K. Kuroki, R. Arita, and H. Aoki, *Phys. Rev. Lett.* **105**, 057003 (2010).
 - ¹⁵ J. Chang, M. Shi, S. Pailh s, M. M nsson, T. Claesson, O. Tjernberg, A. Bendounan, Y. Sassa, L. Patthey, N. Momono, M. Oda, M. Ido, S. Guerrero, C. Mudry, and J. Mesot, *Phys. Rev. B* **78**, 205103 (2008).
 - ¹⁶ G. Ghiringhelli, A. Piazzalunga, C. Dallera, G. Trezzi, L. Braicovich, T. Schmitt, V. N. Strocov, R. Betemps, L. Patthey, X. Wang, and M. Grioni, *Review of Scientific Instruments* **77**, 113108 (2006).
 - ¹⁷ V. N. Strocov, T. Schmitt, U. Flechsig, T. Schmidt, A. Imhof, Q. Chen, J. Raabe, R. Betemps, D. Zimoch, J. Krempasky, X. Wang, M. P. A. Grioni, and L. Patthey, *J. Synchrotron Radiat.* **17**, 631 (2010).
 - ¹⁸ S. Komiya, Y. Ando, X. F. Sun, and A. N. Lavrov, *Phys. Rev. B* **65**, 214535 (2002).
 - ¹⁹ J. Chang, N. B. Christensen, C. Niedermayer, K. Lefmann, H. M. R nnow, D. F. McMorrow, A. Schneidewind, P. Link, A. Hiess, M. Boehm, R. Mottl, S. Pailh s, N. Momono, M. Oda, M. Ido, and J. Mesot, *Phys. Rev. Lett.* **102**, 177006 (2009).
 - ²⁰ A. T. R mer, J. Chang, N. B. Christensen, B. M. Andersen, K. Lefmann, L. M hler, J. Gavilano, R. Gilardi, C. Niedermayer, H. M. R nnow, A. Schneidewind, P. Link, M. Oda, M. Ido, N. Momono, and J. Mesot, *Phys. Rev. B* **87**, 144513 (2013).
 - ²¹ J. Chang, J. S. White, M. Laver, C. J. Bowell, S. P. Brown, A. T. Holmes, L. Maechler, S. Str ssle, R. Gilardi, S. Gerber, T. Kurosawa, N. Momono, M. Oda, M. Ido, O. J. Lipscombe, S. M. Hayden, C. D. Dewhurst, R. Vavrin, J. Gavilano, J. Kohlbrecher, E. M. Forgan, and J. Mesot, *Phys. Rev. B* **85**, 134520 (2012).
 - ²² J. Chang, C. Niedermayer, R. Gilardi, N. B. Christensen, H. M. R nnow, D. F. McMorrow, M. Ay, J. Stahn, O. Sobolev, A. Hiess, S. Pailh s, C. Baines, N. Momono, M. Oda, M. Ido, and J. Mesot, *Phys. Rev. B* **78**, 104525 (2008).
 - ²³ V. Thampy, M. P. M. Dean, N. B. Christensen, L. Steinke, Z. Islam, M. Oda, M. Ido, N. Momono, S. B. Wilkins, and J. P. Hill, *Phys. Rev. B* **90**, 100510 (2014).
 - ²⁴ T. P. Croft, C. Lester, M. S. Senn, A. Bombardi, and S. M. Hayden, *Phys. Rev. B* **89**, 224513 (2014).
 - ²⁵ C. Monney, T. Schmitt, C. E. Matt, J. Mesot, V. N. Strocov, O. J. Lipscombe, S. M. Hayden, and J. Chang, *Phys. Rev. B* **93**, 075103 (2016).
 - ²⁶ J. Lamsal and W. Montfrooij, *Phys. Rev. B* **93**, 214513 (2016).
 - ²⁷ H. Miao, J. Lorenzana, G. Seibold, Y. Y. Peng, A. Amorese, F. Yakhou-Harris, K. Kummer, N. B. Brookes, R. M. Konik, V. Thampy, G. D. Gu, G. Ghiringhelli, L. Braicovich, and M. P. M. Dean, *arXiv* (2016), 1701.00022.
 - ²⁸ L. Braicovich, L. J. P. Ament, V. Bisogni, F. Forte, C. Aruta, G. Balestrino, N. B. Brookes, G. M. De Luca, P. G. Medaglia, F. M. Granozio, M. Radovic, M. Salluzzo, J. van den Brink, and G. Ghiringhelli, *Phys. Rev. Lett.* **102**, 167401 (2009).
 - ²⁹ L. Braicovich, J. van den Brink, V. Bisogni, M. M. Sala, L. J. P. Ament, N. B. Brookes, G. M. De Luca, M. Salluzzo, T. Schmitt, V. N. Strocov, and G. Ghiringhelli, *Phys. Rev. Lett.* **104**, 077002 (2010).
 - ³⁰ M. Guarise, B. D. Piazza, H. Berger, E. Giannini, T. Schmitt, H. M. R nnow, G. A. Sawatzky, J. van den Brink, D. Altenfeld, I. Eremin, and M. Grioni, *Nat Commun* **5**, 5760 (2014).
 - ³¹ M. P. M. Dean, A. J. A. James, A. C. Walters, V. Bisogni, I. Jarrige, M. H cker, E. Giannini, M. Fujita, J. Pellicari, Y. B. Huang, R. M. Konik, T. Schmitt, and J. P. Hill,

- Phys. Rev. B **90**, 220506 (2014).
- ³² Y. Y. Peng, G. Della, M. Minola, M. Conni, A. Amorese, D. Di Castro, G. M. De Luca, K. Kummer, M. Salluzzo, X. Sun, X. J. Zhou, G. Balestrino, M. L. Tacon, B. Keimer, L. Braicovich, N. B. Brookes, and G. Ghiringhelli, *arXiv* (2016), 1609.05405.
- ³³ L. Hozoi, L. Siurakshina, P. Fulde, and J. van den Brink, *Scientific Reports* **1**, 65 EP (2011).
- ³⁴ M. M. Sala, V. Bisogni, C. Aruta, G. Balestrino, H. Berger, N. B. Brookes, G. M. de Luca, D. D. Castro, M. Grioni, M. Guarise, P. G. Medaglia, F. M. Granozio, M. Minola, P. Perna, M. Radovic, M. Salluzzo, T. Schmitt, K. J. Zhou, L. Braicovich, and G. Ghiringhelli, *New Journal of Physics* **13**, 043026 (2011).
- ³⁵ P. G. Radaelli, D. G. Hinks, A. W. Mitchell, B. A. Hunter, J. L. Wagner, B. Dabrowski, K. G. Vandervoort, H. K. Viswanathan, and J. D. Jorgensen, *Phys. Rev. B* **49**, 4163 (1994).
- ³⁶ C. G. Fatuzzo, Y. Sassa, M. Månsson, S. Pailhès, O. J. Lipscombe, S. M. Hayden, L. Patthey, M. Shi, M. Grioni, H. M. Rønnow, J. Mesot, O. Tjernberg, and J. Chang, *Phys. Rev. B* **89**, 205104 (2014).
- ³⁷ J. Chang, M. Månsson, S. Pailhès, T. Claesson, O. J. Lipscombe, S. M. Hayden, L. Patthey, O. Tjernberg, and J. Mesot, *Nature Communications* **4**, 2559 (2013).
- ³⁸ M. Platié, J. D. F. Mottershead, I. S. Elfimov, D. C. Peets, R. Liang, D. A. Bonn, W. N. Hardy, S. Chiuazbalian, M. Falub, M. Shi, L. Patthey, and A. Damascelli, *Phys. Rev. Lett.* **95**, 077001 (2005).
- ³⁹ D. C. Peets, J. D. F. Mottershead, B. Wu, I. S. Elfimov, R. Liang, W. N. Hardy, D. A. Bonn, M. Raudsepp, N. J. C. Ingle, and A. Damascelli, *New Journal of Physics* **9**, 28 (2007).
- ⁴⁰ H. Sakakibara, H. Usui, K. Kuroki, R. Arita, and H. Aoki, *Phys. Rev. B* **85**, 064501 (2012).
- ⁴¹ D. Meyers, H. Miao, A. C. Walters, V. Bisogni, R. S. Springell, M. d'Astuto, M. Dantz, J. Pellicciari, H. Huang, J. Okamoto, D. J. Huang, J. P. Hill, X. He, I. Božović, T. Schmitt, and M. P. M. Dean, *arXiv* (2016), 1612.00890.
- ⁴² J. P. Locquet, J. Perret, J. Fompeyrine, E. Machler, J. W. Seo, and G. Van Tendeloo, *Nature* **394**, 453 (1998).
- ⁴³ M. Abrecht, D. Ariosa, D. Cloetta, S. Mitrovic, M. Onellion, X. X. Xi, G. Margaritondo, and D. Pavuna, *Phys. Rev. Lett.* **91**, 057002 (2003).

VII. APPENDIX A

Here we describe the spin-excitation dispersion of the Heisenberg Hamiltonian derived from the $t - t' - t'' - U$ Hubbard model in two steps. We first consider the simplest model where $t' = t'' = 0$ before including higher order hopping terms.

Generally the dispersion takes the form:

$$\omega(k) = Z\sqrt{A_k^2 - B_k^2}$$

where Z is a renormalization factor. When the Hubbard model contains only the nearest-neighbor hopping integral t , we expand A_k and B_k to second order in t :

$$A_k = A_0 + A_1 + \dots \quad \& \quad B_k = B_0 + B_1 + \dots \quad (2)$$

To express A_i and B_i , we define: $J_1 = \frac{4t^2}{U}$ and $J_2 = \frac{4t'^4}{U^3}$. Moreover we set:

$$P_j(q_h, q_k) = \cos jq_h a + \cos jq_k a \quad (3)$$

$$X_j(q_h, q_k) = \cos jq_h a \cdot \cos jq_k a \quad (4)$$

$$X_{3a}(q_h, q_k) = \cos 3q_h a \cdot \cos q_k a + \cos q_h a \cdot \cos 3q_k a, \quad (5)$$

where $j = 1, 2, 3$, or 4. With this notation we have:

$$A_0 = 2J_1 \quad \& \quad B_0 = -J_1 P_1 \quad (6)$$

and

$$A_1 = J_2(-26 - 8X_1 + P_2) \quad \& \quad B_1 = 16J_2 P_1 \quad (7)$$

When the zone boundary dispersion is defined by $E_{ZB} = \omega(1/2, 0) - \omega(1/4, 1/4)$, one finds $E_{ZB} = 12ZJ_2$. Therefore, a zone boundary dispersion is only found when second order terms J_2 are included. Notice also that since $P_1(1/2, 0) = P_1(1/4, 1/4) = 0$, the B -terms are not contributing to the zone boundary dispersion.

Now let us include second-nearest- t' and third-nearest-neighbor t'' hopping integrals. This involves several additional contributions to A_k and B_k :

$$A_k = A_0 + A_1 + A'_0 + A''_0 + A'_c + A'_1 + A''_c + A''_1 \quad (8)$$

$$B_k = B_0 + B_1 + B'_c. \quad (9)$$

To express these new terms, we introduce the following notation $J'_1 = \frac{4t'^2}{U}$, $J'_2 = \frac{4t'^4}{U^3}$, $J''_1 = \frac{4t''^2}{U}$ and $J''_2 = \frac{4t''^4}{U^3}$. Geometrically the following contributions correspond to different hopping path combinations including the cyclic ones.

$$A'_0 = 2J'_1(X_1 - 1) \quad \& \quad A''_0 = J''_1(P_2 - 2) \quad (10)$$

$$A'_c = -\frac{8J_1}{U^2}(-t'^2 + 4t't'' - 2t''^2)(P_2 - 2) \quad (11)$$

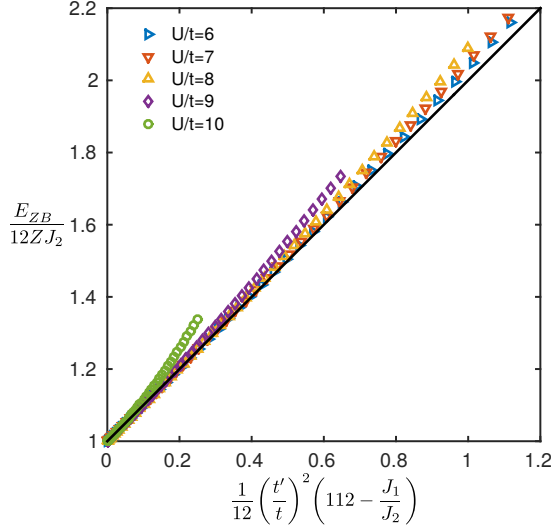


FIG. 5. (Color online) Zone boundary dispersion E_{ZB} normalized to $12ZJ_2$ and plotted versus $\frac{1}{12}(112 - J_1/J_2)(t'/t)^2$. Data points are exact numerical solutions of the Hubbard model for values several of U/t (as indicated) and $t'' = -t'/2$. The solid line is the approximated analytical solution for $U/t = 8$.

$$B'_c = -\frac{4J_1}{U^2} [(6t'^2 - 4t't'')(X_1 - 1) + 3t''^2(P_2 - 2)] P_1 \quad (12)$$

$$A'_1 = 2J'_2(X_2 + 4X_1 - 2P_2 - 1) \quad (13)$$

$$A''_c = \frac{2J'_1J''_1}{U} (-3X_2 + 2X_1 + 5P_2 - X_{3a} - 7) \quad (14)$$

$$A''_1 = J''_2(P_4 - 8X_2 + 4P_2 - 2) \quad (15)$$

As B'_c scales with P_1 , it is again found that B_k does not contribute to the zone boundary dispersion. In Fig. 6, we show the numerical evaluation of E_{ZB} for realistic

$\text{La}_{2-x}\text{Sr}_x\text{CuO}_4$	U (eV)	U/t	t'/t	t''/t	Z	Ref.
$x = 0$	2.2	7.4	0	0	1.18	6 and 7
$x = 0$	3.6	8.3	-0.313	0.167	1.219	8
$x = 0$	3.9	9.1	-0.308	0.154	1.219	★
$x = 0.12$	2.8	6.5	-0.389	0.195	1.219	★
Bi2201						
$x = 0$	3.4	8.0	-0.352	0.176	1.219	★

TABLE I. Parametrization – using the Hubbard model – of the spin-excitation dispersion of LCO^{6,7}, LSCO $x = 0.12$ (this work) and Bi2201³². (★) Values obtained from the fit using the same procedure as described in this appendix, which thus can be directly compared.

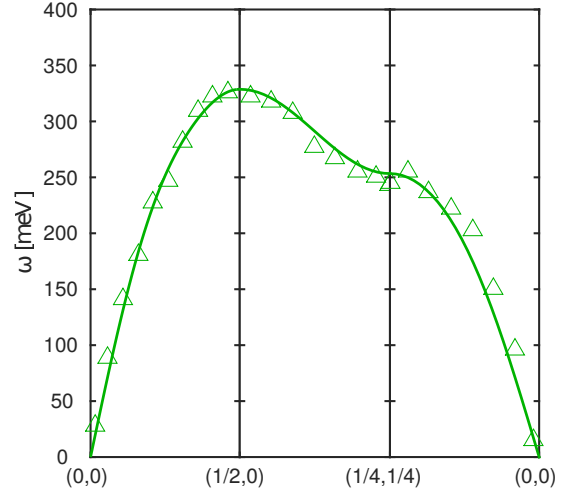


FIG. 6. Spin excitation spectrum of Bi2201 from Ref. 32. The solid line is a fit to the $t - t' - t'' - U$ Hubbard model.

values of U/t , t'/t and with $t'' = -t'/2$. When neglecting terms scaling with J'_2 , J''_2 and $J'_1J''_1$, only Eq. 10 and 11 contribute. Using $P_2(1/2, 0) = 2$, $P_2(1/4, 1/4) = -2$, $X_1(1/2, 0) = -1$ and $X_1(1/4, 1/4) = 0$, we find:

$$\frac{E_{ZB}}{12ZJ_2} \approx 1 + \frac{1}{12} \left(112 - \frac{J_1}{J_2}\right) \left(\frac{t'}{t}\right)^2. \quad (16)$$

This approximation is valid as long as:

$$\frac{U}{t} \geq \sqrt{\frac{28 + 112 \left(\frac{t'}{t}\right)^2}{2 + 3 \left(\frac{t'}{t}\right)^2}}, \quad \text{and} \quad \left|\frac{t'}{t}\right| \lesssim 0.686. \quad (17)$$

As shown in Fig. 5, this analytical expression is a good approximation to the full numerical calculation. Thus it is justified to neglect terms scaling with J'_2 , J''_2 and $J'_1J''_1$ for a realistic cuprate values of U/t and t'/t .

VIII. APPENDIX B

Now, having derived the spin-excitation dispersion within the $t - t' - t'' - U$ Hubbard model, it is possible to fit the experimentally observed dispersion. A final comment goes to the prefactor Z . It is found that, including higher order hopping integrals t' and t'' , Z has a slowly varying momentum dependence. To simplify our analysis we used the mean value obtained⁸ in the first Brillouin zone for the half filled compound La_2CuO_4 . We thus have $Z = 1.219$ constant. From ARPES^{36,37} experiments and LDA calculations¹¹ we have that $t = 0.43$ eV and $t'' = -t'/2$. Our fitting parameters are thus U and t' . In this fashion we obtain a good description of the spin-excitation dispersion of LCO and LSCO $x = 0.12$ (see Fig. 2). The obtained values are given in Table I. In Fig. 6 and Table I, we display in addition our fit and

associated fit parameters from the spin-excitation spectrum measured on Bi2201 (Ref. 32). With these values of U and t' , the relation – shown in Fig. 4 – between E_{ZB} and t' is established.